

https://doi.org/10.1070/QEL17609

Acceleration of electrons in hollow glass capillaries under the action of intense picosecond laser pulses

V.A. Flegentov, K.V. Safronov, D.S. Gavrilov, A.G. Kakshin, N.A. Pkhaiko, A.V. Potapov

Abstract. **The generation of relativistic electron beams in hollow glass capillaries is investigated using a picosecond laser system. A plasma is formed in a capillary due to the ablation of its inner walls by a specially formed pre-pulse. Electron beams with an opening angle of ~40 mrad, exponential energy spectrum with maximum energy about 20 MeV, and a total charge of ~0.2 nC are experimentally detected.**

Keywords: *picosecond laser pulse, pre-pulse, hollow capillary, relativistic electrons, magnetic electron spectrometer.*

1. Introduction

Bremsstrahlung X-ray sources based on laser-plasma electron accelerators have good temporal (several picoseconds) and spatial (several hundred micrometres) characteristics [1, 2] for scientific, commercial, and medical purposes. However, the low output of these sources limits their application range.

Higher irradiation doses can be obtained by increasing the number of electrons accelerated in the laser plasma and by reducing the angular divergence of generated beams [3]. In this context, a promising approach is laser-plasma acceleration in capillary targets [4]. These targets make it possible to form an axisymmetric plasma with a radial density profile, which may facilitate (under certain conditions) laser pulse transmission through a plasma and electron density near the axis. Generally, to form an accelerating medium in a capillary, it is previously filled with a gas through specially drilled channels [5, 6]; another way is to fill the entire target chamber with a gas [7]. The former approach is difficult to implement for target design considerations. A drawback of the latter way is that the presence of a gas medium between the focusing objective and target may lead to self-focusing of a high-power laser beam even before entering a capillary and, therefore, hinder efficient energy transfer into it. In particular, this effect may explain the low charge of electron beams (about 1 pC) in [7]. Kitagawa et al. [8] reported a simpler way of forming an accelerating medium: to use the ablation of inner walls of a hollow gold cone installed before the input end face of capillary. They demonstrated generation of an electron beam with energy up to 100 MeV; the total charge was estimated to be 13 nC (on the assumption that the opening angle of the electron beam is equal to the laser beam convergence angle from the focusing objective to the target).

In this paper, we report the results of successful application of an even simpler design of a capillary target (without an input conical head). An accelerating medium was formed due to the irradiation of capillary inner walls by a specially generated picosecond pre-pulse. Collimated electron beams with energies up to 22 MeV and a total charge up to ~0.2 nC were detected in experiments.

2. Experimental

Experiments were performed on a picosecond Nd : glass laser system with a centre radiation wavelength $\lambda = 1054$ nm, pulse duration $\tau = 0.8-1$ ps, and energy up to 15 J. A beam with a diameter $D = 120$ mm was concentrated in the plane of a capillary target input end face using an off-axis parabolic mirror (PM) with a focal length $F = 200$ mm ($F/D = 1.7$). In the Gaussian optics approximation, the waist diameter in the focus is $d = 4\lambda/\pi(F/D) \approx 2$ μm (at the level of $1/e^2$), and the Rayleigh length is $L_R = \pi d^2/(4\lambda) = 3.5$ μm. Under these conditions, the radiation power density in the waist was $(2-4) \times 10^{19}$ W cm^{-2}.

Formation of laser pre-pulses. To implement electron acceleration, a hollow capillary was previously filled with ablation plasma (formed by an ultrashort pre-pulse). The pre-pulse was generated prior to beam introduction into the main acceleration channel, according to the scheme presented in Fig. 1. The pre-pulse amplitude was controlled using a system of beam splitters with reflection coefficients providing ratios of the main pulse and pre-pulse energies of 10 : 1, 100 : 1, or 1000 : 1. Up to the target, the pre-pulse propagated along the same optical path as the main pulse. The delay of the main pulse arrival at the target was fixed at a level of 1.4 ns.

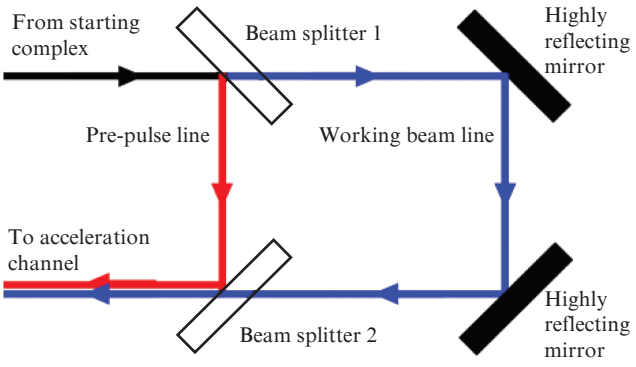

Figure 1. Schematic diagram of pre-pulse formation.

V.A. Flegentov, K.V. Safronov, D.S. Gavrilov, A.G. Kakshin, N.A. Pkhaiko, A.V. Potapov Russian Federal Nuclear Center, Zababakhin All-Russia Research Institute of Technical Physics, ul. Vasil'eva 13, 456770 Snezhinsk, Chelyabinsk region, Russia; e-mail:dep5@vniitf.ru, avp65gr@rambler.ru

Received 13 July 2021
Kvantovaya Elektronika **51** (9) 846–849 (2021)
Translated by Yu.P. Sin'kov

Target unit. Capillary targets were prepared from borosilicate glass of C89-1 grade (72.0% SiO_2); they had the form of hollow tubes with inner diameters w equal to 50, 100, or 140 μm. The capillary wall thickness was equal to the channel diameter, and the capillary length l varied from 2 to 10 mm. The squared ratio $(l/w)^2$ for all targets exceeded the $(F/D)^2$ value for the focusing parabola by a factor of more than 70; thus, the fraction of the pre-pulse energy absorbed by inner capillary walls was no less than 98%.

Before the experiments the capillary axis was carefully aligned with the laser beam axis using a target unit having five degrees of freedom. It provided linear target displacement in three orthogonal directions, as well as rotation around the vertical and horizontal axes. The laser beam was focused in the plane of the capillary end face with an error of ±10 μm; the transverse deviation of the beam waist from the channel centre did not exceed 5 μm, and the angle between the beam and capillary axes was no more than 1 and 5 mrad for target lengths of 10 and 2 mm, respectively.

Measurements of accelerated electron beam characteristics. A schematic of the experiments is presented in Fig. 2. The energy spectrum of accelerated electrons was measured using a magnetic spectrometer based on plane-parallel permanent NdFeB magnets. The spectrometer was located at a distance of 250 mm from the target. A schematic of the spectrometer is presented in Fig. 3. A flexible photoluminescence screen Image Plate (IP BAS-MS), mounted as shown in Fig. 3, played the role of an electron detector. Electrons with energies from 0.9 to 4.5 MeV, transmitted through the input diaphragm (∅1 mm), were focused near the surface detector on the AB segment, where the spectrometer energy resolution, determined by the detector spatial resolution (~100 μm), was less than 1%. Electrons with energies above 7 MeV were recorded on the CD segment. The spectrometer energy resolution on this segment was determined by the input diaphragm diameter; it was about 7% for 25-MeV electrons. The IP sensitivity to electrons with energies above 1 MeV was determined in [9–11]; it barely depends on the electron energy.

To determine the electron beam opening angle, an IP screen 140 mm in diameter, with a hole facing the input diaphragm, was mounted on the front surface of the magnetic spectrometer (see Figs 2 and 3). The screen size in this detection geometry corresponded to an aspect angle of ~30°. The front surface of the IP film was coated by 100-μm-thick Ni foil to ensure protection from laser radiation and low-energy X rays.

The time-integrated luminescence from the region of interaction between the laser pulse and capillary targets was recorded by a 8-bit side CCD camera (see Fig. 2) in the vicinity of second harmonic wavelength (527 nm). The spatial resolution of the detection system was 12 μm.

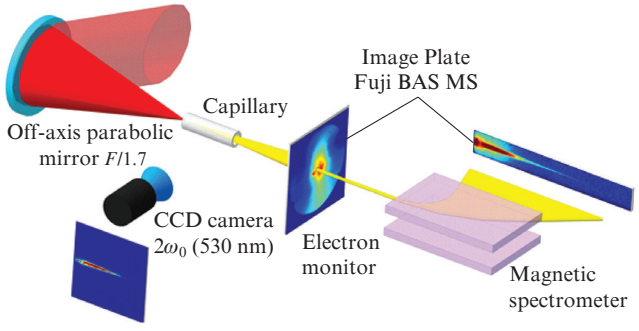

Figure 2. Schematic of experiments on laser-plasma acceleration of electrons from hollow glass capillaries.

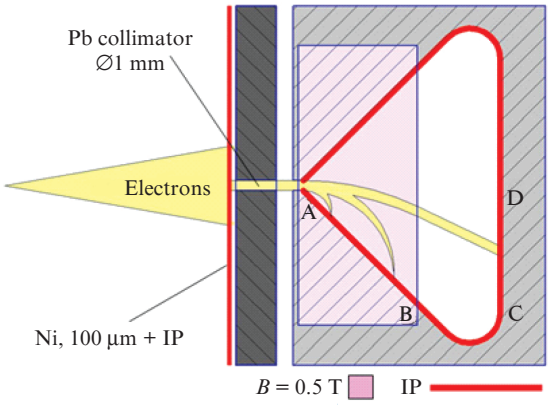

Figure 3. Schematic of the magnetic electron spectrometer.

3. Experimental results

Filling a capillary with ablation plasma. The formation of ablation plasma in capillaries was investigated using single picosecond pulses. The pulse energies were 9 mJ, 90 mJ, and 1.25 J; these values approximately correspond to the specified levels of pre-pulse energies relative to the fundamental radiation with energy of ~10 J. In these experiments the capillary inner diameter and length l were, respectively, 50 μm and 10 mm. Figure 4 shows images of plasma luminescence in capillaries, recorded with a side CCD camera. The laser pulse in the images propagates from left to right. White lines indicate the outer contour of capillaries, constructed from the images recorded before the irradiation.

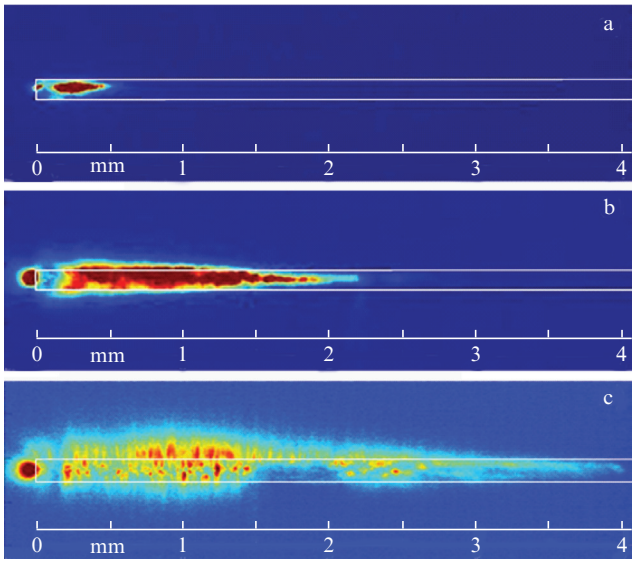

Figure 4. (Colour online) Images of plasma luminescence in capillaries (their external contours are indicated by white lines for clarity) with an inner channel ∅50 μm, obtained using a side CCD camera at laser pulse energies of (a) 9 mJ (without attenuation); (b) 90 mJ (without attenuation); and (c) 1.25 J, with additional luminescence attenuation (using neutral filters) by a factor of ~300.

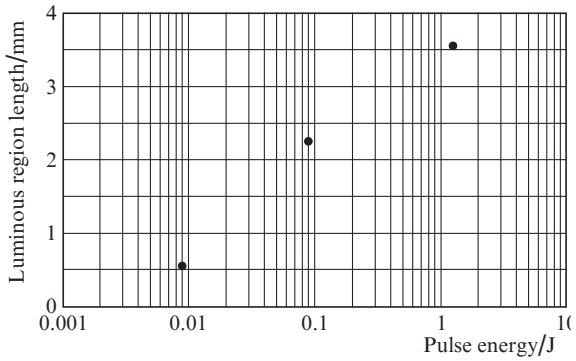

Figure 5. Dependence of the length of the luminous region in capillary on the laser pulse energy (error 5%).

There is an extended region of luminous plasma inside the capillaries, whose length depends on the laser pulse energy. This dependence (Fig. 5) is close to logarithmic.

All images contain a bright spot at the capillary input, near the laser beam waist. Its origin is apparently related to the specific features of Thomson scattering, whose brightness on the second harmonic is $I_{\mathrm{Tscat}} \sim n_e^2 I_{\mathrm{las}}$, where n_e is the plasma density and I_{las} is the intensity of scattered laser radiation. The scattered radiation brightness decreases significantly in the focal spot region; the reason is that, despite the high laser beam intensity in this region, the scattering-medium (plasma) volume is small, and the medium is rarefied. A decrease in the second-harmonic luminescence brightness in the focal spot was also observed in other studies [12]. The rounded shape of the luminescence spot at the capillary input is explained by the detection of total radiation scattered by axisymmetric volume.

Measurements of relativistic electron beam parameters. The electron energy distribution $\mathrm{d}^2N_e/(\mathrm{d}E\mathrm{d}\Omega)$ was determined from the spectrograms recorded with a magnetic spectrometer. All experimentally detected electron beams had an exponential energy spectrum with effective distribution temperature T_{eff} in the range of 0.5–2.8 MeV.

The total electron beam charge Q_{beam} was calculated from the imprints recorded on the IP photoluminescence screen placed before the spectrometer. To this end, the total brightness of electron beam imprint was compared with the image brightness in the vicinity of spectrometer input diaphragm, for which the corresponding charge is known ($\int[\mathrm{d}^2N_e/(\mathrm{d}E\mathrm{d}\Omega)] \times \mathrm{d}E$) from the magnetic spectrometer measurements. Note that the reported estimate assumes that the electron energy is independent of the observation angle. Therefore, determina-

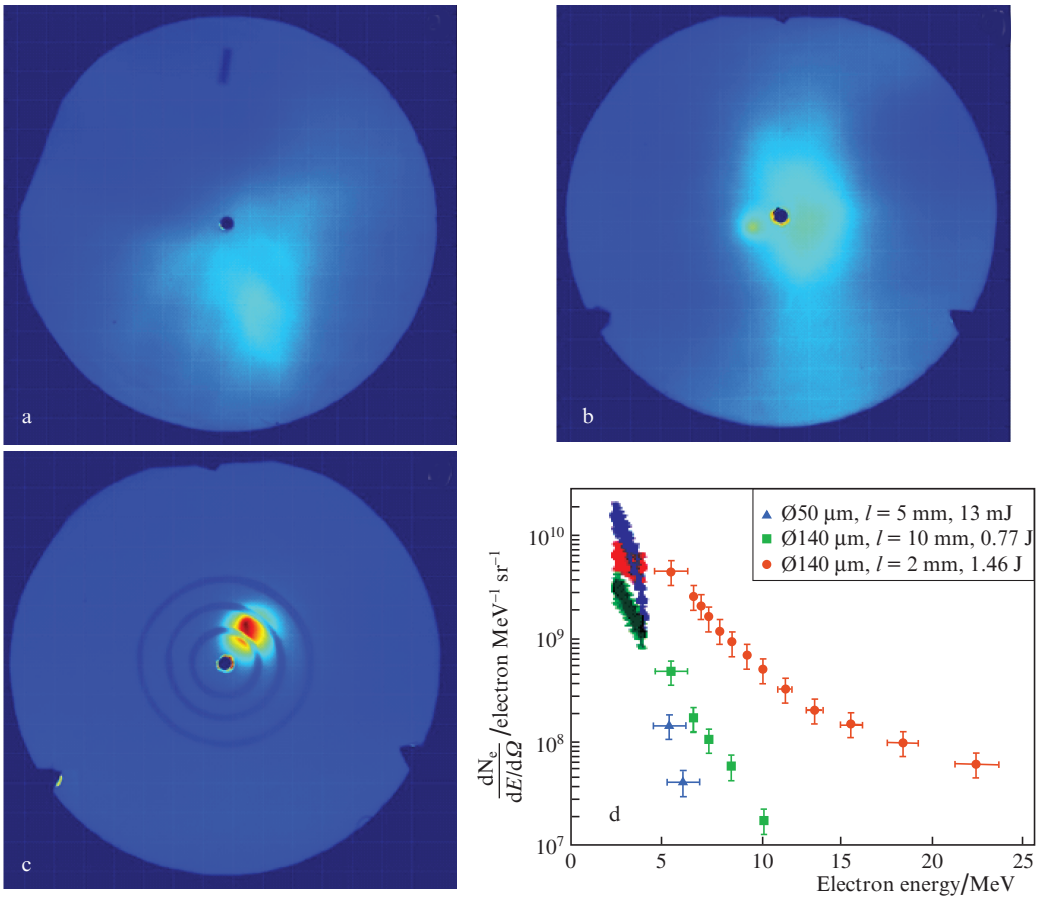

Figure 6. (Colour online) (a–c) Electron beam images from an Image Plate screen installed before the magnetic electron spectrometer: (a) capillary Ø50 μm, $l = 5$ mm, pre-pulse energy 13 mJ; (b) capillary Ø140 μm, $l = 10$ mm, pre-pulse energy 0.77 J; and (c) capillary Ø140 μm, $l = 2$ mm, pre-pulse energy 1.46 J. (d) Energy spectra of electrons accelerated towards the spectrometer input diaphragm. The grid in images (a–c) has a step of 1 cm, which corresponds to an opening angle of ~40 mrad near the spectrometer diaphragm. The spectra were recorded in the same experiments as the images (a–c).

tion of Q_{beam} by the aforementioned method may lead to significant errors in experiments where beams exhibit a nonuniform angular distribution.

Figure 6 shows examples of electron beam imprints for acceleration from capillary targets of different sizes at different pre-pulse energies. The corresponding electron energy spectra obtained from magnetic spectrometer measurements are shown in Fig. 6d. The concentric rings of lower brightness in Fig. 6c are due to the shadow from the marks of 300-μm-thick lead foil, installed before the IP screen in this experiment. These marks are used to take into account the contribution from X-ray quanta to the image when calculating the total electron beam charge. The marks are transparent for electrons with energies above 1 MeV but absorb low-energy X rays from the laser plasma. The screen illumination in the mark shadow is observed only in the regions of electron beam arrival. All experiments with 5- and 10-mm-long capillaries are characterised by a highly nonuniform angular distribution of beam electrons (Figs 6a and 6b). The total beam charges are estimated to be 30–50 pC. The experiments showed that, with an increase in the capillary diameter, the requirements to the pre-pulse energy for successful generation of relativistic electrons become more stringent. For example, for capillaries with ∅50 μm acceleration occurs at a pre-pulse energy of ~10 mJ, whereas for capillaries with ∅140 μm one needs ~1 J laser energy to form a plasma medium with properties appropriate for acceleration.

The best results were obtained for capillary targets with ∅140 μm and 2 mm long, at a pre-pulse energy of 1.2–1.5 J. An electron beam imprint recorded in one of such experiments is presented in Fig. 6c. It can be seen that the beam is collimated and has a bell-shaped angular distribution with a divergence of ~20 mrad (FWHM). The total opening angle of generated beam corresponds approximately to the capillary aspect ratio (the ratio of the diameter of capillary to its length). This conclusion is in agreement with the results of [7]. The maximum electron energy is 22 MeV, and the total charge is 200 ± 50 pC.

Figure 7 shows an image recorded by the side CCD camera in the experiment with collimated beam acceleration from a capillary with ∅140 μm and $l = 2$ mm, at a pre-pulse energy of 1.46 J. It is noteworthy that most intense luminescence is observed at the capillary output, a fact indicating that a significant part of the laser pulse passed throughout the capillary.

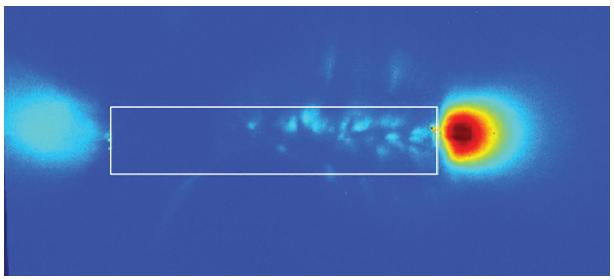

Figure 7. (Colour online) Image obtained with a side camera in the experiment with acceleration of collimated electron beam in a capillary with ∅140 μm and $l = 2$ mm, at a pre-pulse energy of 1.46 J. The capillary external contour is indicated by a white line. The laser pulse propagates from left to right. The image was recorded with additional attenuation (using neutral filters) by a factor of 240.

4. Conclusions

Experiments on generation of relativistic electrons from capillary targets were performed on a picosecond laser system. An acceleration plasma channel was formed in a capillary due to the ablation of its inner walls using a specially formed ultrashort pre-pulse.

It is found experimentally that, for each value of capillary inner diameter in the range of 50–140 μm, there is an optimal pre-pulse energy at which accelerated electrons are observed.

It is found that, for capillaries with an inner diameter of 140 μm, a decrease in the capillary length from 10 to 2 mm leads to significant improvement of the electron beam quality and an increase in the accelerated particle energy. Beams with an opening angle of ~40 mrad, exponential energy spectrum with a peak at about 22 MeV, and a total charge of ~200 pC were detected in experiments with these capillaries.

References

1. Courtois C., Edwards R., Compant La Fontaine A., et al. *Phys. Plasmas*, **20**, 083114 (2013).
2. Glinec Y., Faure J., Le Dain L., et al. *Phys. Rev. Lett*., **94**, 025003 (2005).
3. Edwards R.D., Sinclair M.A., Goldsack T.J., et al. *Appl. Phys. Lett*., **80** (12), 25 (2002).
4. Compant La Fontaine A., Courtois C., Lefebvre E. *Phys. Plasmas*, **19**, 023104 (2012).
5. Leemans W.P., Nagler B., Gonsalves A.J., et al. *Nat. Phys*., **696**, 2 (2006).
6. Ju J., Svensson K., Ferrari H., Döpp A., et al. *Phys. Plasmas*, **20**, 083106 (2013).
7. Mori Y., Sentoku Y., Kondo K., et al. *Phys. Plasmas*, **16**, 123103 (2009)
8. Kitagawa Y., Sentoku Y., Akamatsu Sh., et al. *Phys. Rev. Lett*., **92**, 205002 (2004).
9. Zeil K., Kraft S.D., et al. *Rev. Sci. Instrum*., **81**, 013307 (2010).
10. Boutoux G., Rabhi N., Batani D., et al. *Rev. Sci. Instrum*., **86**, 113304 (2015).
11. Rabhi N., Bohacek K., Batani D., et al. *Rev. Sci. Instrum*., **87**, 053306 (2016).
12. Najmudin Z., Dangor A.E., Modena A., et al. *IEEE Trans. Plasma Sci*., **28** (4), 1057 (2000).